communications physics

ARTICLE

https://doi.org/10.1038/s42005-023-01430-7 OPEN

Direct numerical evidence of the Phillips initial stage and its antecedent during wind-wave generation

Tianyi Li [1] & Lian Shen [1]✉

How wind generates ocean surface waves is a classic fluid mechanics problem, and it is commonly believed that the resonance mechanism between wind and surface waves, first proposed by Phillips in 1957, is responsible for the early stages of wind-wave generation. However, there has not been any conclusive study to fully validate this theory. We present the results of a combined theoretical and computational study of the initial response of a calm water surface to turbulent wind and an analysis in terms of the Phillips theory on wind-wave generation. We address a nascent stage of wind-wave generation after the sudden impact of a turbulent wind on a calm water surface but before the initial stage described by Phillips. We show that in such nascent stage, the wave energy grows over time following a quartic law. We provide direct numerical evidence of the resonance mechanism during the initial stage and clarify its role in the formation of the heterogeneous wave energy distribution in the spectral space.

[1] Department of Mechanical Engineering and St. Anthony Falls Laboratory, University of Minnesota, Minneapolis, MN 55455, USA. ✉email: shen@umn.edu

Determining the manner in which wind generates waves has been a profound problem of great interest to the scientific community for over half a century[1–3] and has attracted more and more attention in recent years[4–7]. A comprehensive understanding of wind–wave interactions is crucial to many areas of research, such as global climate change, ocean environment, and offshore engineering research[8–11]. The presence of ocean waves influences the flow motions in the upper ocean and the exchange of soluble gases (e.g., carbon dioxide) between the atmosphere and the ocean[12]. Wind blowing is a major source for the evolution and growth of ocean waves, of which the amplitude and patterns are distinct at different stages of wave growth[13].

Extensive efforts have been applied toward understanding the mechanisms of wind–wave interactions over decades. Most studies focus on interactions between wind and prescribed surface waves of finite amplitude when ocean surface waves have already been generated by the wind; these momentum and energy transfer processes have been thoroughly studied in theoretical, computational, and experimental approaches[3,14–19]. However, information about wave evolution in the early stage of the wind-wave generation process remains elusive. A fundamental question to be addressed is how surface waves arise from a calm water surface exposed to turbulent wind.

In 1957, Phillips proposed a theory to model the role of turbulent wind in the growth of surface waves from an initially flat water surface[2]. A key observation is the different time scales of the wave motions and air pressure fluctuations at the water surface. The wave motion time scale, quantified by the inverse angular frequency $\Lambda^{-1}(\boldsymbol{k})$ at wavenumber $\boldsymbol{k}$, shows the dispersive nature of surface waves. The time scale of air pressure fluctuation development, denoted by Θ, is longer than the time scale of surface wave motions in water, i.e., $\Theta > \Lambda^{-1}$. When the elapsed time of surface wave development is less than Θ, i.e., $t < \Theta$, air pressure fluctuations at the air–water interface are advected downstream at the convection velocity according to Taylor's frozen turbulence hypothesis[20]. When the timescale is much longer than Θ, i.e., $t \gg \Theta$, the turbulent structures in the airflow change, and the space–time correlation in air pressure fluctuations should be taken into account when modeling the long-term behavior of the pressure and wave fields.

Phillips theory predicts two main stages in wave generation after a turbulent airflow blows over a calm water surface, namely, an initial stage and a principal stage. The initial stage corresponds to the times between the wave motion time scale Λ^{-1} and air pressure fluctuation development time scale Θ, i.e., $\Lambda^{-1} < t < \Theta$. During this stage, the air pressure fluctuations excite surface waves through a resonance mechanism[2]. Resonance takes place between surface waves on water and turbulent air pressure fluctuations when the convection velocity of air pressure fluctuations matches the wave phase velocity at a certain wavenumber, which leads to an initial excitation of surface deformation. For the surface wave components that satisfy the resonance condition, the surface wave energy grows quadratically over time. The principal stage occurs when the elapsed time far exceeds the pressure fluctuation development time scale, i.e., $t \gg \Theta$. Air pressure fluctuations decorrelate with themselves over time, upon which Taylor's frozen hypothesis breaks down[21,22]. The wave energy asymptotically grows linearly over time[2,6]. After the wave amplitude grows further and begins to affect the airflow, the shear instability mechanism associated with the critical layer proposed by Miles[3] and the sheltering mechanism proposed by Belcher and Hunt[14] is responsible for the exponential growth of the wave energy with time. The exponential growth rate yielded by Miles' theory can also be obtained using uniform asymptotic approximations[18]. Recently, a new theoretical model[7] based on the Orr–Sommerfeld equation and a wave sheltering mechanism was developed to describe the multistage evolution of water waves after the emergence of the exponential growth stage. We note that recent experimental research[7,23] also studied the initial stages of wind-wave evolutions. The initial stage in our study refers to the specific stage predicted by the Phillips theory[2], where the resonance mechanism plays a crucial role.

It is commonly believed that the initial and principal stages of Phillips theory provide a plausible explanation for the early evolution of surface waves under a turbulent wind. Some recent progress has been made in validating and characterizing the principal stage theory. Numerical simulations[4,6] and laboratory experiments[5] have confirmed the linear growth of the surface elevation variance, which is proportional to the wave energy, in the period that corresponds to the principal stage in Phillips theory. With the aid of direct numerical simulations (DNS) of the wind-wave generation process, we recently proposed a random sweeping turbulence pressure–wave interaction model[6] to quantitatively predict the wave growth rate during the principal stage of Phillips theory. The second-order and high-order moments of surface elevation exhibit power-law growth with time in this stage[24].

However, no conclusive studies have been conducted on wave dynamics before the principal stage described by Phillips theory. A thorough comprehension of Phillips' initial stage (when the time scale is between that of wave motion and air pressure fluctuation development time scale, i.e., $\Lambda^{-1} < t < \Theta$) and the preceding stage (when the time scale is smaller than the wave motion time scale, i.e., $t < \Lambda^{-1}$) can complement current understanding of how waves are initially generated by a turbulent wind on a calm water surface.

In this study, we perform the DNS of the wind-wave generation process and analyze the results to obtain direct numerical evidence for the resonance mechanism described in the initial stage of Phillips theory. We report direct evidence for the quadratic growth of wave energy near the resonance condition in the initial stage. We also discover its antecedent, namely, a nascent stage ($t < \Lambda^{-1}$), when the wave energy grows quartically over time. Moreover, this study assesses the contributions of pressure and shear stress of the airflow at the water surface to the initial growth of surface waves. Finally, we elucidate the role played by the resonance mechanism in the development of a heterogeneous wave energy spectrum from an initially unidirectional field.

Results

The nascent stage of wind-generated waves. In this subsection, we focus on simulation results that were obtained during the nascent stage preceding the initial stage described in the Phillips theory. The initial stage in Phillips theory corresponds to $\Lambda^{-1} < t < \Theta$[2]. We first focus on the evolution of interface deformation from a flat surface in response to a sudden imposition of turbulent airflow, before the initial stage, $0 < t < \Lambda^{-1}$, which remains unclear in Phillips theory. We call this period the nascent stage. An ideally flat air–water interface is improbable in nature, but this setup is crucial to understanding the early response of surface deformation to turbulent airflow and seeking the origin of wind-generated ocean waves.

The effect of an initial disturbance at the interface and the wave growth mechanism can be isolated according to the following analysis. Owing to the small magnitude of the deformation of the free surface, this deformation can be analyzed using a linearized surface wave framework. We can consider the free evolution of an initial wave disturbance and the generation of waves by air forcing. For the former, the system conserves energy over time when viscous dissipation is neglected[25]. If an initial disturbance is

present, $\eta|_{t=0} = \eta_0$ and $\partial_t\eta|_{t=0} = \eta_0'$, then the temporal evolution of the surface elevation η is constrained by $\|\eta\|_{L_x^2}(t) \le \|\eta_0\|_{L_x^2} + \|\Lambda^{-1}\eta_0'\|_{L_x^2}$. Here, $\Lambda(\boldsymbol{k}) = \sqrt{g|\boldsymbol{k}| + \sigma|\boldsymbol{k}|^3/\rho^w}$ denotes the dispersion relation of surface waves in the Fourier space, g is the gravity acceleration, σ is the surface tension between air and water, and ρ^w is the water density. Λ is treated as a Fourier multiplier when acting on variables in physical space. The unit of Λ is s^{-1}, and Λ can be considered as the inverse of the time scale. To conclude, if there is no air forcing, then the evolution of the initial deformations is bounded over time by the functionals of the initial wave field. Therefore, it is acceptable to consider a flat water surface at the initial time when studying wind-wave growth. The setup of an initially calm water surface helps us understand the fundamental mechanism of the very early stage of wind-wave generation. This numerical setup reproduces the initial condition of the prominent Phillips theory[2] in wind-wave generation and has also been adopted in other numerical studies[4,19]. Similarly, experimental studies[7,23] also studied wind-wave evolution starting from an initially quiescent water surface. At the very beginning of the wind-wave generation process, the surface elevation is so small that it can be considered as a small wrinkle. In this study, we uniformly utilize the term wave to refer to the surface deformation at various wind-wave generation stages, which is consistent with the notation in the original Phillips theory[2].

As the wave amplitudes increase from zero, we can further decompose the surface elevation and water velocity into components induced by pressure fluctuations and those induced by shear stress fluctuations at the air–water interface. For finite-amplitude water waves, it is well understood that the effect of air pressure on wave growth is more significant than that of air shear stress at the water surface. Nevertheless, the comparison between pressure-induced waves and shear stress-induced waves in wind-wave generation is not trivial, because both arise from a flat interface. Many theories of wind-wave generation assume that the shear stress effect is negligible[2,3]. The validity of this assumption should be evaluated during the entire early stage of the wind-wave generation process.

Taking advantage of the numerical scheme, we can control the forcing effect at the interface for a mechanistic study. The fully coupled scheme provides both the turbulent air pressure and the shear fluctuations at the air–water interface. These effects can be isolated by applying only the pressure or the shear stress on the water surface. Thus, we can numerically investigate the specific contributions of air pressure and shear fluctuations to wave growth. The water waves are generated by turbulent airflow without any assumptions of preexisting initial disturbances of the water surface. Figure 1 provides an illustration of the surface deformation and flow field shortly after turbulent airflow is imposed over a calm water surface.

Next, we investigate whether the air-pressure-induced waves indeed consistently dominate the air-shear-stress-induced waves. We decompose the contributions from the air pressure fluctuations and the shear stress fluctuations to the wave growth based on linearized water wave theory. First, we focus on air-pressure-induced wave growth. The governing equation for surface elevation can be expressed as[2] (see Supplementary Note 1 in the Supplementary Material for the detailed derivations):

$$\partial_{tt}\eta + \Lambda^2\eta = -\frac{1}{\rho^w} D_0 p(\boldsymbol{x}, t), \tag{1}$$

where ρ^w denotes the water density and D_0 is the Dirichlet-to-Neumann operator. Given a function $f(\boldsymbol{x})$ and its Fourier transform $\widehat{f}(\boldsymbol{k})$, $D_0 f(\boldsymbol{x})$ is defined as $\widehat{D_0 f} = |\boldsymbol{k}|\widehat{f}$. We consider the $t \to 0$ limit of Eq. (1), which corresponds to the early response

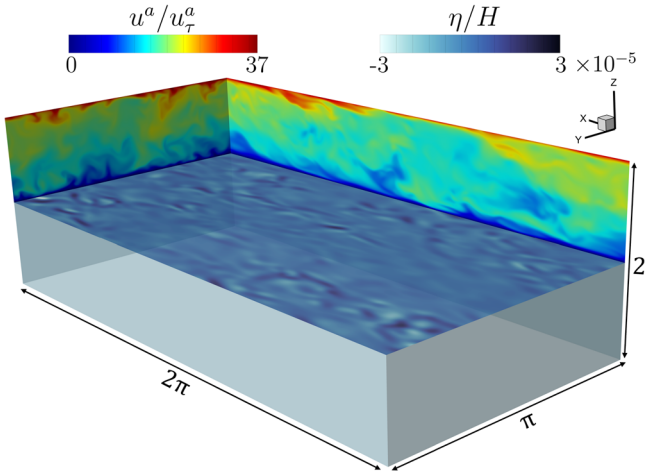

Fig. 1 Three-dimensional air–water interface deformation and air velocity field. This illustration depicts the instantaneous flow field shortly after the wind-wave generation process starts ($t = 0.015H/u_\tau^a$). The contours on two representative vertical planes show the streamwise velocity u^a in the air domain. The horizontal contours show the wave elevation η. Normalization is based on the air domain height H and air friction velocity u_τ^a. The computational domains on the air and water sides have the same size $(L_x, L_y, L_z) = (2\pi, \pi, 1)$, which is normalized by the air domain height H. The x-axis corresponds to the airflow direction, and the (x, y) plane is horizontal and periodic in both x- and y-directions.

of surface waves after a turbulent wind blows over a calm water surface. The limiting behavior of the surface elevation in the spectral space, $\hat{\eta}$, leads to power-law growth of surface elevation variance, $|\hat{\eta}(\boldsymbol{k}, t)|^2 = (4\rho^{w2})^{-1}k^2|\hat{p}|^2t^4 + O(t^6)$. Keeping the leading-order term and taking the inverse Fourier transform, we obtain a quartic power law for surface elevation variance in the nascent stage,

$$\left\langle \eta_p^2 \right\rangle = \frac{\left\langle |D_0 p|^2 \right\rangle t^4}{4\rho^{w2}}. \tag{2}$$

In the original Phillips theory[2], a time-dependent response factor was introduced to separate a quartic function of time from the wave energy spectrum component in the initial stage when the time is larger than the wave period (see Eq. (3.5) in ref. [2]). Our present analysis indicates that this response factor has a finite limit that does not depend on the time in the nascent stage and the quartic growth dominates when the time approaches zero.

We next analyze the evolution of shear-induced waves. Owing to the low viscosity of water, viscous diffusion due to the external shear stress occurs within a thin boundary layer underneath the water surface, and diffusion is much faster in the vertical than the horizontal direction. Under these conditions, the linearized shear stress balance at the free surface is $\nabla_h \cdot \boldsymbol{\tau} = -\rho^w \nu^w \partial_{zz} w$, where $\nabla_h = (\partial_x, \partial_y)$ is the horizontal nabla operator, $\boldsymbol{\tau}$ is the shear stress exerted on the water surface, ν^w is the water viscosity, and w is the vertical velocity. In the framework of linear wave theory, we include the vertical diffusion term in the w-momentum equation and introduce the shear effect into the wave evolution equation (see Supplementary Note 1 in the Supplementary Material for detailed derivations):

$$\partial_{tt}\eta + \Lambda^2\eta = -\frac{1}{\rho^w} \nabla_h \cdot \boldsymbol{\tau}(\boldsymbol{x}, t). \tag{3}$$

Equation (3) describes the wave dynamics subject to the shear stress fluctuations of airflow and is consistent with the recent spectral theory of viscous surface deformation[26] when the viscous damping effect is neglected. Taking the limit as $t \to 0$, we obtain

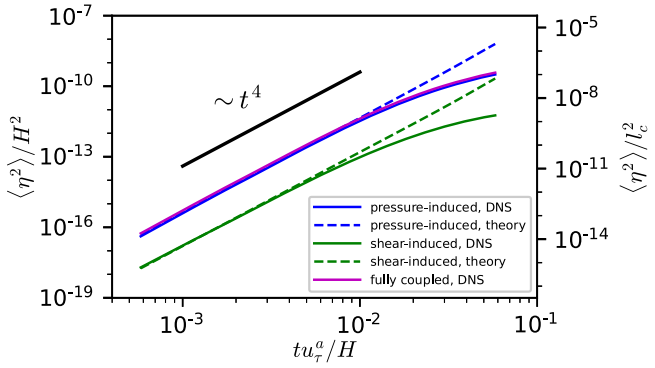

Fig. 2 Wave growth behavior in the nascent stage. Initial growth of pressure-induced (blue) and shear-induced (green) surface elevation variance $\langle \eta^2 \rangle$, normalized using the air domain height H and the capillary length scale $l_c = \sqrt{\sigma/(\rho^w g)}$ on the left and right y-axes, respectively. The wave growth of the fully coupled simulation when both pressure and shear fluctuations are considered is shown in the magenta line. Solid lines and dashed lines represent the direct numerical simulation (DNS) results and theoretical predictions, respectively.

quartic power-law growth of the shear-induced surface deformation variance,

$$\langle \eta_s^2 \rangle = \frac{\langle |\nabla_h \cdot \boldsymbol{\tau}|^2 \rangle t^4}{4\rho^{w2}}. \tag{4}$$

We further validate the above theoretical analysis of the wave dynamics in the nascent stage using the numerical simulation results. Figure 2 shows a comparison of the above analytical solutions, Eqs. (2) and (4), with the DNS results for the pressure-induced and shear-induced waves. The DNS results confirm that $\langle \eta_p^2 \rangle$ and $\langle \eta_s^2 \rangle$ both follow quartic power-law growth in the nascent stage. In the current numerical simulations, a smaller time step is utilized compared to the previous literature on wind-wave generation[4], with the present time step being only one-fifth of the previous value. This reduction in time step can accurately capture wave growth dynamics in the very early stage. Our numerical simulations reveal a consistent trend of quartic growth of surface elevation variance during the interval $tu_\tau^a/H = (0, 0.01)$ in the nascent stage. This stage contains more than three hundred time steps in our simulations. The quartic growth law remains evidently prominent during the nascent stage. For the first thirty largest wavenumbers in the range of $kl_c = (0.056, 1.68)$ that the DNS can resolve, the inverse of wave angular frequencies normalized by the air friction velocity and domain height, i.e., $\Lambda^{-1} u_\tau^a/H$, varies between 0.115 and 0.011. Therefore, the duration for this nascent stage varies between 0.1 and 1 times the inverse of wave angular frequencies for different wavenumbers. As shown in Fig. 2, in the fully coupled simulation, the surface elevation variance also follows a quartic growth behavior during the nascent stage, taking into account the combined effects of pressure and shear stress. The pressure-induced quantity can be considered the dominant component of surface elevation.

From the beginning of the wind-wave generation process, the pressure-induced surface elevation variance is consistently more than 50 times larger than the shear-induced surface elevation variance. The conducted DNS method resolves all turbulence scales but has challenges in simulating larger length or velocity scale problems (i.e., larger Reynolds number) owing to the computational cost. Nevertheless, this result holds as the Reynolds number further increases. In wall-bounded turbulence, the statistics of wall pressure fluctuations normalized using the wall units slightly increase with increasing Reynolds number[27], while the statistics of wall shear stress fluctuations in the wall units are invariant with the Reynolds number[28]. We numerically examined an important assumption in Phillips theory[2]: the early development of surface waves is a passive response of the water surface to the air pressure forcing, and the contribution from the turbulent shear stress is assumed to be negligible. From the results shown above, we conclude that such an assumption is still valid in the limit where the elapsed time approaches zero.

The resonance mechanism in the initial stage. Next, we focus on the wave evolution characteristics in the initial stage of Phillips theory and provide numerical evidence of the existence of its initial stage. In the initial stage, when the time scale is $\Lambda^{-1} < t < \Theta$, a resonance mechanism is assumed to be responsible for the wave growth according to Phillips theory[2]. Despite the theoretical achievement that has been well-known for decades, comprehensive experimental or numerical evidence to validate this mechanism remains elusive to date. In the initial stage, pressure fluctuations are convected with velocity $\boldsymbol{U}$ according to Taylor's frozen turbulence hypothesis. In Fourier spectral space, the governing equations of water waves in the presence of a turbulent wind can be expressed as

$$\partial_{tt}\hat{\eta}(\boldsymbol{k}, t) + \Lambda(\boldsymbol{k})^2 \hat{\eta}(\boldsymbol{k}, t) = -\frac{1}{\rho^w} \exp(-i\boldsymbol{k} \cdot \boldsymbol{U}t)\hat{p}(\boldsymbol{k}, 0), \tag{5}$$

resulting in $|\hat{\eta}(\boldsymbol{k}, t)|^2$ evolving as[2]:

$$|\hat{\eta}(\boldsymbol{k}, t)|^2 = \frac{k^2 |\hat{p}|^2}{2\rho^{w2}\Lambda^4(\alpha^2 - 1)^2} \big(\alpha^2 - 2(\alpha + 1)\cos(\Lambda(\alpha - 1)t) + 2(\alpha - 1)\cos(\Lambda(\alpha + 1)t) - (\alpha^2 - 1)\cos(2\Lambda t) + 3\big). \tag{6}$$

Here, the variable $\alpha = \boldsymbol{k} \cdot \boldsymbol{U}/\Lambda$ denotes the ratio of the convection velocity of turbulent pressure fluctuations projected in the $\boldsymbol{k}$-direction to the wave phase velocity. In Eq. (6), $|\hat{\eta}|^2$ is continuously dependent on $\alpha \in (0, \infty)$. Note that $\alpha = 1$ is a point of continuity. At $\alpha = 1$, the wave's phase speed equals the pressure convection speed, and the wave energy spectrum component grows as $|\hat{\eta}|^2 \sim t^2$, which was first predicted by Phillips[2]. For $\alpha = 1 + \epsilon$, where ϵ is a small perturbation, we obtain:

$$|\hat{\eta}(\boldsymbol{k}, t)|^2 = \frac{k^2 |\hat{p}|^2}{8\rho^{w2}\Lambda^4} \big(2\Lambda^2 t^2 + 1 - 2\Lambda t \sin(2\Lambda t) - \cos(2\Lambda t)\big) + O(\epsilon). \tag{7}$$

Equation (7) above directly indicates the quadratic growth of $|\hat{\eta}(\boldsymbol{k}, t)|^2$ associated with the resonance mechanism in the initial stage.

Next, we provide an elucidation of the resonance mechanism from the dynamic perspective of the temporal global maxima of wave energy spectrum components. As shown in Eq. (6), the wave energy spectrum components $|\hat{\eta}|^2$ at different wavenumbers consist of three harmonic functions with distinct oscillation periods. We focus on a critical time t_c when $|\hat{\eta}|^2$ reaches its global maximum for the first time. Equivalently, at time $t = t_c$, the three harmonic terms in Eq. (6) simultaneously reach their maxima. Near the resonance curve $\chi(\boldsymbol{k}) = \boldsymbol{k} \cdot \boldsymbol{U} - \Lambda(\boldsymbol{k}) = 0$ where α approaches 1, the coefficients of harmonics $\cos(\Lambda(\alpha - 1)t)$ and $\cos(2\Lambda t)$ vanish, but the term $-2(\alpha + 1)\cos(\Lambda(\alpha - 1)t)$ remains and can reach its maximum at $t = \pi/(\Lambda(\alpha - 1))$ for the first time. As such, near the resonance curve $\chi(\boldsymbol{k})$, the critical time t_c can be approximately expressed as $t_c = \pi/(\Lambda(\alpha - 1))$. Note that t_c is singular at $\alpha = 1$. For a wave whose wavenumber is located closer to the resonance curve $\chi(\boldsymbol{k})$, more time is required for the wave energy spectrum component to reach its maximum. Before the time reaches t_c, the wave energy spectrum component grows over

time overall, and its amplitude exhibits oscillatory behavior owing to the modulations by the other harmonics.

When α is far from 1, that is, when $\boldsymbol{k}$ is far from the resonance curve $\chi(\boldsymbol{k}) = \boldsymbol{k}\cdot\boldsymbol{U} - \Lambda(\boldsymbol{k}) = 0$ in the spectral domain, the wave energy spectrum component $|\hat{\eta}(\boldsymbol{k}, t)|^2$ does not monotonically increase over time. Furthermore, using number theory, we prove (see Supplementary Note 2 in the Supplementary Material for details) the existence of a corresponding critical time at which the energy $|\hat{\eta}(\boldsymbol{k}, t)|^2$ decreases below a threshold that can be preselected to be arbitrarily small. We obtain the following general upper bound on a Diophantine approximation from number theory[29]. There exists an infinite number of relatively prime integer pairs (p_i, q_i), $i \in \mathbb{Z}^+$, such that $|(\alpha+1)/2 - p_i/q_i| < 1/q_i^2$. For any arbitrary $\delta > 0$, there exists an integer pair (p_i, q_i) satisfying the following two conditions: $|(\alpha+1)/2 - p_i/q_i| < 1/q_i^2$ and $q_i > 2\pi(\rho^w)^{-1}k|\hat{p}|\Lambda^{-2}|\alpha^2 - 1|^{-1}\delta^{-1/2}$. Thus, by perturbation analysis, we obtain the upper bound of the wave energy spectrum component $|\hat{\eta}|^2$ at $T = \pi\Lambda^{-1}q_i$,

$$|\hat{\eta}(\boldsymbol{k}, T)|^2 < \delta + O(\delta^2). \tag{8}$$

Equation (8) indicates that when $\boldsymbol{k}$ is far from the resonance curve, the wave energy spectrum component can decrease to any arbitrarily small value at some time.

Next, we present the numerical evidence for wind-generated resonance waves and nonresonance waves in the initial stage. Figure 3a depicts the wavenumbers at which the wave energy spectrum component $|\hat{\eta}|^2$ grows over time according to the DNS results. The blue shading denotes the least-squared fitting results of the power index β assuming the wave energy spectrum component behaves as a power-law function of time, i.e., $|\hat{\eta}|^2 \sim t^\beta$. The wave components for which the energy grows quadratically over time are distributed around the resonance curve, which is represented by the red dotted line in the figure. The convection velocity of pressure fluctuations $\boldsymbol{U}$ is computed from the wavenumber–frequency spectrum of air pressure at the water surface. $\boldsymbol{U}$ lies along the x-direction, and its magnitude is expressed as $U = k_x^{-1}\int|\tilde{p}(k_x, k_y, \omega)|^2\omega \mathrm{d}k_y\mathrm{d}\omega / (\int|\tilde{p}(k_x, k_y, \omega)|^2\mathrm{d}k_y\mathrm{d}\omega)$, where $\tilde{p}(k_x, k_y, \omega)$ denotes the space–time Fourier transform of $p(x, y, t)$. The resonance curve $\chi(\boldsymbol{k}) = 0$ is obtained by solving $\boldsymbol{k}\cdot\boldsymbol{U} = \Lambda(\boldsymbol{k})$. Figures 3b, c illustrate two representative wavenumbers $(k_x l_c, k_y l_c) =$ (0.06, 0.22) and (1.18, 2.69), at which the wave energy spectrum components grow over time and the values for the ratio α are 0.9 and 1.2, respectively. The orange dashed lines indicate quadratic growth. Figures 3d, e show two examples of wavenumbers $(k_x l_c, k_y l_c) = (0.06, 4.37)$ and (2.86, 0.34), at which the ratio α is far from 1, being 0.05 and 2.7, respectively. For these two cases, the wave energy spectrum components do not grow but oscillate over time. At certain times, the amplitude of $|\hat{\eta}|^2$ can reach very small values. The DNS results shown in Fig. 3 provide direct evidence of the resonance mechanism in the initial stage of Phillips theory[2]. Our numerical results demonstrate a consistent quadratic growth pattern of the wave energy spectrum components around the resonance curves. This pattern is particularly noticeable within a range of k_x and k_y values where the wavenumber is not excessively large. The underlying reason for this phenomenon is attributed to the pressure fluctuation spectrum, in which the magnitude of the pressure fluctuation component decays as the wavenumber increases. In regions with high wavenumber values, the pressure fluctuation magnitude diminishes significantly. Consequently, the waves resulting from these pressure fluctuations are much smaller than those in regions with low wavenumber values.

The above results show that the temporal evolution of wave energy spectrum components at different wavenumbers exhibits heterogeneous features in the initial stage of wind-wave generation. A thorough understanding of the overall wave growth behavior over time is also crucial. A qualitative study of the evolution of surface elevation variance for all of the wave energy spectrum components combined, $\langle\eta^2\rangle$, was first conducted by Phillips[2]. In physical space, the surface elevation variance can be evaluated via integration over the wave energy spectrum from the Plancherel theorem[30]. By adopting the uniform Jacobian determinant approximation in a resonance curve-based orthogonal coordinate transformation, Phillips predicted that the overall evolution of surface elevation variance is a linear function of time. We obtain the numerical evidence that the surface elevation variance grows linearly over time in the initial stage, as shown in Fig. 4. Shemer[23] experimentally observed a linear wave energy growth in the initial wind-wave generation process. Our numerical approach further reinforces the conclusion and examines the resonance mechanism associated with the initial stage of the wind-wave generation process[2].

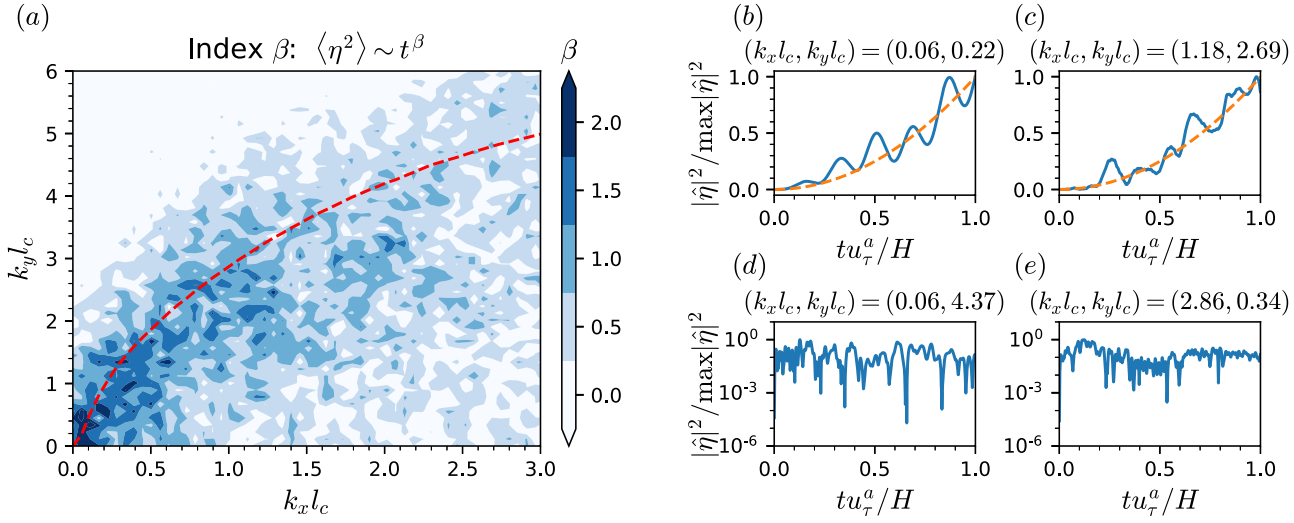

Fig. 3 Spectral variations in the temporal growth of wave energy in the initial stage. a The blue shading represents the magnitude of the index β assuming power-law growth of the wave energy spectrum component, i.e., $\langle\eta^2\rangle \sim t^\beta$, at wavenumber (k_x, k_y). The red dashed line shows the resonance curve $\chi(\boldsymbol{k}) = 0$. **b**, **c** Show two examples in which $|\hat{\eta}|^2$ (blue line) evolves quadratically, and the orange dashed line illustrates the trend $|\hat{\eta}|^2 \sim t^2$. **d**, **e** show two examples in which $|\hat{\eta}|^2$ oscillates over time. The titles of (**b**–**e**) denote the value of the wavenumber (k_x, k_y) in each plot.

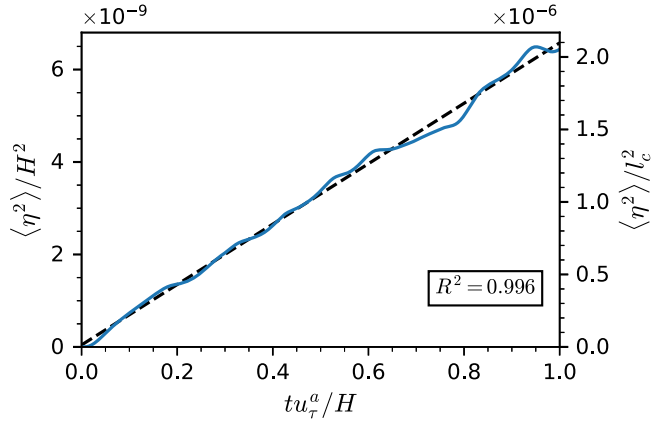

Fig. 4 Overall growth of surface elevation variance $\langle \eta^2 \rangle$ in the initial stage. The surface elevation variance $\langle \eta^2 \rangle$ has all of the wave energy spectrum components combined and is normalized using the air domain height H and the capillary length scale l_c on the left and right y-axes, respectively, in the initial stage. The blue line denotes the DNS results, and the black dashed line shows the linear regression, with the coefficient of determination $R^2 = 0.996$.

Formation of the heterogeneous wave energy spectrum. In this section, we focus on the time evolution of the surface wave energy spectrum. A variety of factors affect the wind-wave spectrum in oceans, such as wind speed, fetch distance, and ocean swells. The Joint North Sea Wave Observation Project (JONSWAP) spectrum and Pierson–Moskowitz spectrum are two well-known parameterizations of the ocean wave spectrum for a developing wind sea and fully developed wind sea, respectively[31,32]. Nevertheless, until now, there has not been a comprehensive explanation of the formation of the wind-sea spectrum during the wind-wave generation process. Here, we describe how an initial surface wave spectrum changes from an omnidirectional spectrum to a heterogeneous spectrum in the early period of wind-wave generation.

We obtain the expression of surface elevation variance in the nascent stage (Eq. (2)) in a perturbative manner when t is near zero. Equation (2) indicates that the surface wave spectrum solely depends on the air pressure spectrum and not on the wave dispersion. When the elapsed time is longer than the wave motion time scale in the initial stage, wave dispersion emerges in the evolution of the wave behavior. The surface elevation spectrum can be viewed as an air pressure spectrum altered by a modification coefficient associated with wave dispersion. Here, we show that the wave energy spectrum component $|\hat{\eta}(\boldsymbol{k})|^2$ has an upper bound over time when it is far from the resonance curve. In the expression for $|\hat{\eta}(\boldsymbol{k})|^2$ in the initial stage (Eq. (6)), owing to the periodicity of the cosine function, we have:

$$|\hat{\eta}|^2(\boldsymbol{k}, t) < \frac{1}{\rho^{w2}} k^2 |\hat{p}|^2 C(\boldsymbol{k}). \tag{9}$$

Here, the modification coefficient $C(\boldsymbol{k}) = 0.5\Lambda^{-4}(\alpha^2 - 1)^{-2}(2|\alpha + 1| + 2|\alpha - 1| + |\alpha^2 - 1| + \alpha^2 + 3)$ has the following piecewise expression:

$$C(\boldsymbol{k}) = \begin{cases} 4((\boldsymbol{k} \cdot \boldsymbol{U})^2 - \Lambda^2)^{-2} & \alpha < 1 \\ \Lambda^{-2}(\boldsymbol{k} \cdot \boldsymbol{U} - \Lambda)^{-2} & \alpha > 1 \end{cases} \tag{10}$$

The value of $C(\boldsymbol{k})$ indicates the discrepancy between the distributions of the wave energy spectrum $|\hat{\eta}|^2$ and the premultiplied pressure fluctuation spectrum $k^2|\hat{p}|^2$. When the wavenumbers are far from the resonance curve, $C(\boldsymbol{k})$ is reduced (Fig. 5d), resulting in the heterogeneity of the wave energy spectrum. Next, we compute the wave energy spectrum at different times during the simulation, as depicted in Figs. 5a–c. Initially, as shown in Fig. 5a, the spectrum is spatially omnidirectional according to the wave dynamics in the nascent stage. The evolution of wave energy spectrum components is primarily related to air pressure fluctuations. As time progresses, the influence of wave dispersion on the distribution of wave energy spectrum components becomes evident in the initial stage (see Figs. 5b, c). In the wavenumber space, the wave energy begins to be accumulated near the resonance curve where the convection velocity of air pressure fluctuations match the wave phase velocity, depicted by the red curve in Fig. 5c, d. Figure 5d visualizes the distribution of the modification coefficient $C(\boldsymbol{k})$ (see Eq. (10)) in the wavenumber space, representing the heterogeneous characteristics arising from wave dispersion. To conclude, the distribution of the wave energy spectrum gradually changes over time, and we observe the formation of spatial heterogeneity along the resonance curve in the initial stage of the wind-wave generation process.

Conclusions

In this study, we conducted DNS of turbulent airflow over an initially calm water surface to investigate how surface waves are initiated. The results show that the shear-induced surface wave fluctuations are consistently bounded by the pressure-induced wave fluctuations when the air–water interface is distorted by the airflow. Moreover, we discover a nascent stage that occurs before the Phillips initial stage. We theoretically predict that the wave elevation variance growth would follow a quartic power law during the nascent stage, and the DNS results confirm this prediction. The motions of surface deformation are governed solely by turbulent airflow when the time elapsed is much shorter than the wave motion time scale. The nascent stage describes the inceptive growth of surface deformation in a perturbative manner. Considering the fact that the magnitude of initially generated surface waves is small, we focused on the linearized Navier–Stokes equations and the stress balance on the air–water interface to explain our numerical findings to the limit of $t = 0$. The analytical solutions can quantitatively describe the numerical results back to the time $t = 0$. This combination of numerical simulations and analytical analysis establishes a comprehensive and self-consistent framework to prove laws about the earliest stages of wave development.

Our simulation provides direct numerical evidence of the resonance mechanism during the initial stage of Phillips theory when the elapsed time is longer than the wave motion time scale but shorter than the air pressure fluctuation development time scale. During the initial stage, the wave energy spectrum components close to the resonance curve in the spectral space evolve quadratically over time. Wave energy spectrum components far from the resonance curve oscillate over time and can reach arbitrarily small values at certain times. When the wavenumber is located away from the resonance curve, the magnitude of the wave energy spectrum component is bounded by a finite value based on Eq. (9). The DNS results show that the overall growth of surface elevation variance exhibits linearity over time, which agrees with the qualitative hypothesis of the initial stage in Phillips theory[2]. As a result of the resonance mechanism, the omnidirectional waves formed in the nascent stage evolve during the initial stage to a heterogeneous wave field in the spectral space. Although evidence has been previously reported in the literature for the subsequent principal stage in Phillips theory[2], the critical layer mechanism[3], and the sheltering mechanism[14], the direct evidence of the resonance mechanism during the initial

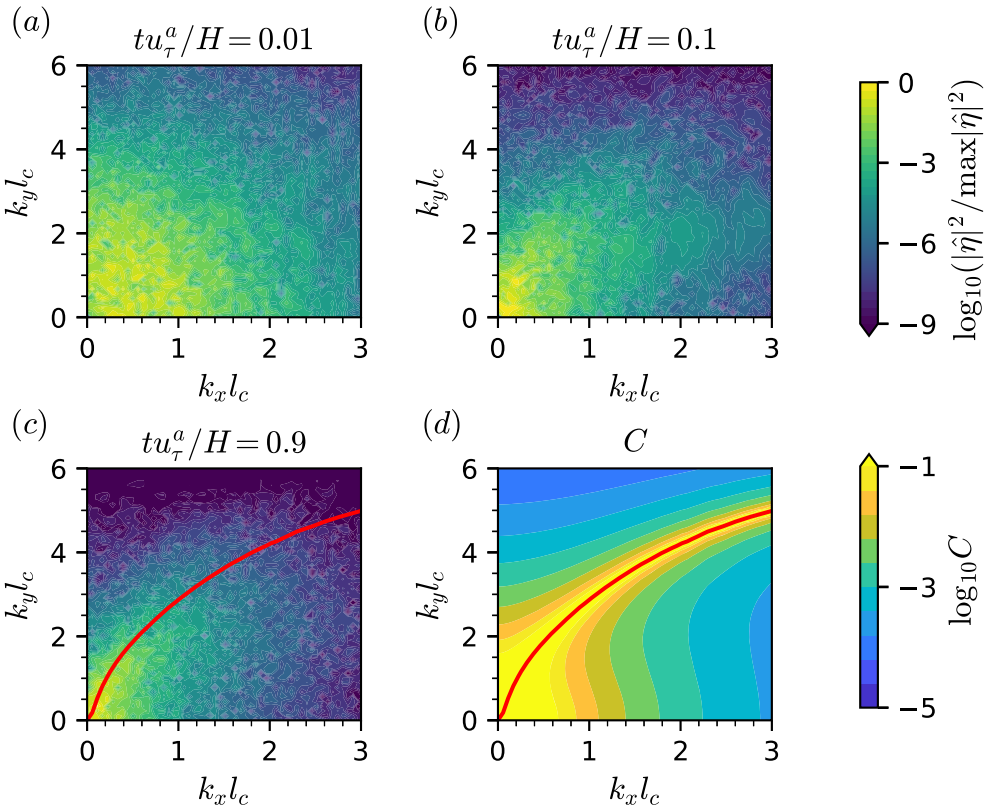

Fig. 5 Temporal evolution of wave energy spectrum components in the wavenumber space. a, **b**, **c** Contours of the wave energy spectrum component $|\hat{\eta}(\boldsymbol{k})|^2$ at $tu_\tau^a/H = 0.01, 0.1$ and 0.9, respectively. **d** Contours of the modification coefficient C, where the contour color is kept the same when $\log_{10} C > -1$ to avoid singularities. The red line is the resonance curve $\chi(\boldsymbol{k}) = 0$.

stage in Phillips theory and the study of the preceding nascent stage are reported in the present paper. The present study focuses on examining the nascent stage and the initial stage of wave evolution. As time increases, wind-generated waves undergo the principal stage[2] and the exponential growth stage[3], as discussed in our previous study[6] which utilized the same physical parameters in the simulation setup. Our study is supportive of the prominent Phillips theory of wind-wave generation[2] during the wind-wave generation process starting from a quiescent water surface till dominant surface waves have been generated.

Methods

Numerical scheme. We conduct numerical simulations using a wave-surface-fitted DNS code developed by our group, which has been extensively used and validated in the previous wind–wave interaction studies[16,33–36]. In the DNS, the air and water motions are governed by the continuity equation and incompressible Navier–Stokes equations:

$$\nabla \cdot \boldsymbol{u} = 0, \tag{11}$$

$$\frac{\partial \boldsymbol{u}}{\partial t} + \boldsymbol{u} \cdot \nabla \boldsymbol{u} = -\frac{1}{\rho}\nabla p + \nu \Delta \boldsymbol{u}. \tag{12}$$

Here, $\boldsymbol{u}$ denotes the velocity vector, p denotes the pressure, ρ denotes the density, and ν denotes the kinematic viscosity of air or water. The computational space is divided into a water domain and an air domain, with their adjacent boundary being the dynamically evolving air–water interface. The air friction velocity is 0.08 m s^{-1}. The physical properties of air and water are set to their values at sea level and a temperature of 15 °C. The air domain height is set to be 0.0489 m, and the streamwise and spanwise domain lengths are 0.307 m and 0.154 m, respectively. These choices were made based on the resolution requirement of DNS, i.e., directly resolving the Kolmogorov scale in the physical problem.

In each domain, Eqs. (11) and (12) are synchronously solved on a curvilinear grid fitting the air–water interface[33]. In the simulation, a grid of 384^3 elements is adopted to discretize both the air and water domains. The continuity of the velocity and the balance of stresses across air–water interface are enforced through an efficient iteration scheme, and the fully nonlinear kinematic and dynamic boundary conditions are imposed at this interface[33]. The computational domain is discretized using a hybrid pseudospectral and finite-difference method. The second-order Adams–Bashforth scheme is used to discretize the convective terms, and the Crank–Nicholson scheme is applied to the viscous terms. A fractional step method is adopted for the time advancement of the Navier–Stokes equations[37]. At each time step, the evolution of surface elevation is calculated using a predictor–corrector method, which is iteratively integrated with the Navier–Stokes solver. The overall numerical accuracy is second-order in both space and time. This choice of the second-order accuracy scheme is recognized as a robust and reliable method for computational fluid dynamics[38]. The scheme chosen is suited for the research of wind–wave interaction and has been used and validated in previous studies[6,35,36]. Especially for the early stages of wind-wave development with small wave amplitudes, the scheme conserves mass and momentum accurately. For example, during the initial stage of wind-wave generation, the relative mean surface elevation normalized by its instantaneous maximum magnitude, defined as $\langle \eta \rangle / \max(\eta)$, is less than 4×10^{-8}. Constant shear stress at the top boundary of the air domain is applied to drive the airflow. We use a no-slip velocity boundary condition at the bottom of the water domain.

Periodic boundary conditions are adopted in horizontal directions. Details of the computational schemes, parameters, and validations are available in Li and Shen[6].

Data availability

Data are available from the corresponding author upon reasonable request.

Code availability

Codes for analyzing data and generating plots are available from the corresponding author upon reasonable request.

Received: 13 April 2023; Accepted: 13 October 2023;
Published online: 24 October 2023

References

1. Ursell, F. Wave generation by wind. Surveys in Mechanics 216–249 (1956).
2. Phillips, O. M. On the generation of waves by turbulent wind. *J. Fluid Mech.* **2**, 417–445 (1957).
3. Miles, J. W. On the generation of surface waves by shear flows. *J. Fluid Mech.* **3**, 185–204 (1957).
4. Lin, M.-Y., Moeng, C.-H., Tsai, W.-T., Sullivan, P. P. & Belcher, S. E. Direct numerical simulation of wind-wave generation processes. *J. Fluid Mech.* **616**, 1–30 (2008).
5. Zavadsky, A. & Shemer, L. Water waves excited by near-impulsive wind forcing. *J. Fluid Mech.* **828**, 459–495 (2017).
6. Li, T. & Shen, L. The principal stage in wind-wave generation. *J. Fluid Mech.* **934**, A41 (2022).
7. Geva, M. & Shemer, L. Excitation of initial waves by wind: a theoretical model and its experimental verification. *Phys. Rev. Lett.* **128**, 124501 (2022).
8. Sullivan, P. P. & McWilliams, J. C. Dynamics of winds and currents coupled to surface waves. *Ann. Rev. Fluid Mech.* **42**, 19–42 (2010).
9. D'Asaro, E. A. Turbulence in the upper-ocean mixed layer. *Ann. Rev. Marine Sci.* **6**, 101–115 (2014).
10. Stevens, R. J. & Meneveau, C. Flow structure and turbulence in wind farms. *Ann. Rev. Fluid Mech.* **49**, 311–339 (2017).
11. Yu, L. Global air–sea fluxes of heat, fresh water, and momentum: energy budget closure and unanswered questions. *Ann. Rev. Marine Sci.* **11**, 227–248 (2019).
12. Jähne, B. & Haußecker, H. Air-water gas exchange. *Ann. Rev. Fluid Mech.* **30**, 443–468 (1998).
13. Young, I. R. Wind generated ocean waves (1999).
14. Belcher, S. & Hunt, J. Turbulent shear flow over slowly moving waves. *J. Fluid Mech.* **251**, 109–148 (1993).
15. Sullivan, P. P., McWilliams, J. C. & Moeng, C.-H. Simulation of turbulent flow over idealized water waves. *J. Fluid Mech.* **404**, 47–85 (2000).
16. Cao, T. & Shen, L. A numerical and theoretical study of wind over fast-propagating water waves. *J. Fluid Mech.* **919**, A38 (2021).
17. Carpenter, J., Buckley, M. & Veron, F. Evidence of the critical layer mechanism in growing wind waves. *J. Fluid Mech.* **948**, A26 (2022).
18. Bonfils, A., Mitra, D., Moon, W. & Wettlaufer, J. Asymptotic interpretation of the Miles mechanism of wind-wave instability. *J. Fluid Mech.* **944**, A8 (2022).
19. Cimarelli, A., Romoli, F. & Stalio, E. On wind–wave interaction phenomena at low Reynolds numbers. *J. Fluid Mech.* **956**, A13 (2023).
20. Taylor, G. I. Production and dissipation of vorticity in a turbulent fluid. *Proceedings of the Royal Society of London. Series A-Mathematical and Physical Sciences* **164**, 15–23 (1938).
21. Del Alamo, J. C. & Jiménez, J. Estimation of turbulent convection velocities and corrections to Taylor's approximation. *J. Fluid Mech.* **640**, 5–26 (2009).
22. Geng, C. et al. Taylor's hypothesis in turbulent channel flow considered using a transport equation analysis. *Phys. Fluids* **27**, 025111 (2015).
23. Shemer, L. On evolution of young wind waves in time and space. *Atmosphere* **10**, 562 (2019).
24. Li, T. & Shen, L. Evolution of wave characteristics during wind-wave generation. In *Proceedings of 34th Symposium on Naval Hydrodynamics* (2022).
25. Zakharov, V. E. Stability of periodic waves of finite amplitude on the surface of a deep fluid. *J. Appl. Mech. Tech. Phys.* **9**, 190–194 (1968).
26. Perrard, S., Lozano-Durán, A., Rabaud, M., Benzaquen, M. & Moisy, F. Turbulent windprint on a liquid surface. *J. Fluid Mech.* **873**, 1020–1054 (2019).
27. Choi, H. & Moin, P. On the space-time characteristics of wall-pressure fluctuations. *Phys. Fluids A: Fluid Dyn.* **2**, 1450–1460 (1990).
28. Mathis, R., Marusic, I., Chernyshenko, S. I. & Hutchins, N. Estimating wall-shear-stress fluctuations given an outer region input. *J. Fluid Mech.* **715**, 163–180 (2013).
29. Dirichlet, L. Verallgemeinerung eines satzes aus der lehre von den kettenbrüchen nebst einigen anwendungen auf die theorie der zahlen. *SB Preuss. Akad. Wiss* **1842**, 5–16 (1842).
30. Plancherel, M. & Leffler, M. Contribution à l'étude de la représentation d'une fonction arbitraire par des intégrales définies. *Rendiconti del Circolo Matematico di Palermo (1884-1940)* **30**, 289–335 (1910).
31. Hasselmann, K. et al. Measurements of wind-wave growth and swell decay during the joint north sea wave project (JONSWAP).Ergaenzungsheft zur Deutschen Hydrographischen Zeitschrift, Reihe A (1973).
32. Pierson Jr, W. J. & Moskowitz, L. A proposed spectral form for fully developed wind seas based on the similarity theory of S.A. Kitaigorodskii. *J. Geophys. Res.* **69**, 5181–5190 (1964).
33. Yang, D. & Shen, L. Simulation of viscous flows with undulatory boundaries: Part II. Coupling with other solvers for two-fluid computations. *J. Comput. Phys.* **230**, 5510–5531 (2011).
34. Yang, D. & Shen, L. Direct numerical simulation of scalar transport in turbulent flows over progressive surface waves. *J. Fluid Mech.* **819**, 58–103 (2017).
35. Hao, X. & Shen, L. Wind–wave coupling study using LES of wind and phase-resolved simulation of nonlinear waves. *J. Fluid Mech.* **874**, 391–425 (2019).
36. Cao, T., Deng, B.-Q. & Shen, L. A simulation-based mechanistic study of turbulent wind blowing over opposing water waves. *J. Fluid Mech.* **901**, A27 (2020).
37. Kim, J. & Moin, P. Application of a fractional-step method to incompressible Navier-Stokes equations. *J. Comput. Phys.* **59**, 308–323 (1985).
38. Huynh, H., Wang, Z. J. & Vincent, P. E. High-order methods for computational fluid dynamics: a brief review of compact differential formulations on unstructured grids. *Computers Fluids* **98**, 209–220 (2014).

Acknowledgements

This work was supported by the Office of Naval Research.

Author contributions

L.S. proposed the study. T.L. performed the analyses and calculations under the supervision of L.S. T.L. and L.S. wrote and reviewed the manuscript.

Competing interests

The authors declare no competing interests.

Additional information

Supplementary information The online version contains supplementary material available at https://doi.org/10.1038/s42005-023-01430-7.

Correspondence and requests for materials should be addressed to Lian Shen.

Peer review information *Communications Physics* thanks Oleg Druzhinin and the other, anonymous, reviewer(s) for their contribution to the peer review of this work.

Reprints and permission information is available at http://www.nature.com/reprints

Publisher's note Springer Nature remains neutral with regard to jurisdictional claims in published maps and institutional affiliations.